Journal of Industrial and Engineering Chemistry 20 (2014) 46–53

Contents lists available at SciVerse ScienceDirect

Journal of Industrial and Engineering Chemistry

journal homepage: www.elsevier.com/locate/jiec

Ethanol to hydrocarbons using silver substituted polyoxometalates: Physicochemical and catalytic study

Mohamed Mokhtar, Sulaiman N. Basahel, Tarek T. Ali *

Chemistry Department, Faculty of Science, King Abdulaziz University, P.O. Box 80203, 21589 Jeddah, Saudi Arabia

ARTICLE INFO

Article history:
Received 6 October 2012
Accepted 20 April 2013
Available online 28 April 2013

Keywords:
$Ag_xH_{3-x}PMo_{12}O_{40}$
Keggin structure
Raman spectroscopy
Acid catalysis
Ethanol dehydration
Ethylene selectivity

ABSTRACT

Thermally stable and insoluble silver salts of 12-molybdophosphoric acid with varying amount of Ag cations were prepared. XRD results indicated the presence of single phase of $Ag_xH_{3-x}PMo_{12}O_{40}$ ($0 < x < 3$). FTIR and Raman results indicated that Ag was incorporated in the secondary structure of Keggin ion. The catalytic conversion of ethanol increased in the order of $H_3PMo > Ag_2PMo > Ag_1PMo > Ag_3PMo$. Pure H_3PMo is highly selective to dimethyl ether formation; in contrast $Ag_xH_{3-x}PMo_{12}O_{40}$ catalysts offered better ethylene selectivity. The pyridine adsorption studies revealed that increase of Ag incorporating led to increase the Lewis acid sites.

1. Introduction

The utilization of ethanol from biomass fermentation instead of petroleum as chemical feedstock is considered as an alternative process that attracts the research worldwide. This alternative pathway could share in the reduction of CO_2 emission from the industries. Bio-ethanol is an attractive alternative feedstock to be used for the production of ethylene and diethyl ether. Ethylene is one of the major feedstock of the petrochemical industry. Production of petrochemicals from a non-petroleum, environmentally friendly feedstock and development of new, efficient ethylene production processes are considered as challenging research areas [1–3].

Aliphatic alcohols, with exception of methanol, have two modes of dehydration; bi-molecular dehydration to produce ethers and intra molecular dehydration to olefins as represented in Eqs. (1) and (2):

$$2CH_3CH_2OH \rightarrow CH_3CH_2OCH_2CH_3 + H_2O \quad (1)$$

$$CH_3CH_2OH \rightarrow CH_2 = CH_2 + H_2O \quad (2)$$

Both dehydration reactions of alcohols to give ethers and olefins are well known acid catalyzed reactions which proceed over different solid acid catalysts such as H-mordenites, H-ZSM-5, H-beta zeolite and silica-alumina [4,5].

Heteropolyacid (HPA) catalysts were considered in the dehydration reaction of alcohols due to their higher activity than the conventional solid acid catalysts [6–8]. Recently, Ciftci et al. [9] applied tungstophosphoric acid impregnated MCM-41 catalysts for alcohol dehydration reaction. They observed 99.9% ethylene selectivity at 300 °C, with about 98% ethanol conversion. However, proton containing HPAs are highly soluble in polar and non-polar solvents, which retard their use as industrial heterogeneous catalysts.

It is well known that the protons in the secondary structure of HPA can be exchanged partially or completely with different metal cations (e.g., Cs^+, NH_4^+, and Ag^+) without affecting the primary Keggin structure to prevent the HPA being leached. The catalytic behaviour of HPA metal salts attracts considerable interest, due to their multi-functional behaviour [10]. These salts are efficient in most of the reactions proceeded by acidic catalyzed processes [11]. The primary influence on the activity for alcohols to hydrocarbons is the concentration and strength of Brönsted acid centres presented in metal salts of HPAs [12].

Gurgul et al. [13] studied the effect of humidity on catalytic performance and stability of $Ag_3PW_{12}O_{40}$. The authors observed that $Ag_3PW_{12}O_{40}$ offered 99.8% ethylene selectivity and 70% ethanol conversion at 2% humidity and 220 °C reaction temperature. With the increase of humidity to 9%, the selectivity to ethylene was lowered to 99.2% at the same reaction temperature, but ethanol conversion was increased to 100%.

* Corresponding author. Permanent address: Chemistry Department, Faculty of Science, Sohag University, Sohag 82524, Egypt. Tel.: +966 2 6400000/68987; fax: +966 2 6952292.
E-mail addresses: ttali@kau.edu.sa, catalysa98@yahoo.com (Tarek T. Ali).

1226-086X/$ – see front matter © 2013 The Korean Society of Industrial and Engineering Chemistry. Published by Elsevier B.V. All rights reserved.
http://dx.doi.org/10.1016/j.jiec.2013.04.028

Thus, the authors concluded that the presence of water stabilized the surface composition of $Ag_3PW_{12}O_{40}$. Matachowski et al. [14] reported the eco-friendly production of ethylene by dehydration of ethanol reaction using $Ag_3PW_{12}O_{40}$ salt in nitrogen and air atmospheres.

Although, $Ag_3PW_{12}O_{40}$ has demonstrated high catalytic ability for the dehydration of ethanol to ethylene, its high acidity reduces its stability. In our previous study, we prepared copper salts of H_3PMo and the incorporation of copper resulted in an increase of the selectivity towards diethyl ether formation [15]. Motivated by the aforementioned findings, and our ongoing endeavours in the development of selective catalyst for ethylene production from ethanol, we report Ag-substituted H_3PMo solid acid catalysts for the selective dehydration of ethanol into ethylene. To best of our knowledge, the application of partially and fully Ag substituted H_3PMo catalysts for the aforementioned reaction has not previously been reported.

2. Material and methods

2.1. Materials

12-Molybdophosphoric acid ($H_3PMo_{12}O_{40}{\cdot}29H_2O$) (SD Fine Chemicals, India) and $AgNO_3$ (Sigma–Aldrich, UK) were the starting materials to synthesize Ag-substituted H_3PMo salts. Ethanol 99.8% produced by BDH chemicals (USA) for preparative gas chromatograph (GC) was used as a reactant. Pyridine 99.9% produced by BDH chemicals (USA) for spectrophotometric measurements used as adsorptive material.

The catalysts of $Ag_xH_{3-x}PMo_{12}O_{40}$, (where x = 1, 2 and 3) were prepared by previously described procedures [16]. Stoichiometric amounts of aqueous silver nitrate salt were added slowly, by means of a burette, to an aqueous solution of 12-molybdophosphoric acid with constant stirring. The yellowish white precipitate was formed and it was aged in water bath for 72 h at 40 °C. The dried powder was obtained after evaporation of solutions to dryness at 100 °C. All the samples were calcined at 300 °C for 3 h, in a static air atmosphere.

The sample code name was designed in the following code names: 12-molybdophosphoric acid = H_3PMo, $Ag_1PMo = AgH_2PMo_{12}O_{40}$, $Ag_2PMo = Ag_2HPMo_{12}O_{40}$ and $Ag_3PMo = Ag_3PMo_{12}O_{40}$.

2.2. Techniques

Thermogravimetric (TG) and differential scanning calorimetry (DSC) analyses were carried out on computerized Shimadzu Thermal Analyzer TA60 Apparatus (Japan). A Ceramic sample boat was used for TGA analysis. Sample weighing 10 ± 0.1 mg was heated up to 1000 °C at 10 °C min^{-1} in a flow of 40 ml min^{-1} O_2 gas. For the DSC measurement, samples weighing 5 ± 0.1mg was heated up to 500 °C at 10 °C min^{-1} in a flow of 40 ml min^{-1}. X-ray powder diffractograms were recorded using a Bruker diffractometer (Bruker D8 advance target). Ni-filtered Cu Kα radiation (λ = 1.541838 Å) was used as a constant source of radiation. The generator was operated at 35 kV and 20 mA, and diffractometer at 2° diverting and receiving slits and a scan rate of 20 mm min^{-1}. FTIR spectra were obtained by the KBr disc technique in the wavelength range 4000–400 cm^{-1}, using Perkin Elmer Spectrum 100 FT-IR spectrometer spectrophotometer, the number of scans is 40, and resolution 4 cm^{-1}. The Raman spectra of samples were measured with a Bruker Equinox 55 FT-IR spectrometer equipped with a FRA106/S FT-Raman module and a liquid N_2 cooled Ge detector, using the 1064 nm line of an Nd:YAG laser with an output laser power of 200 mW. Thermo Scientific Evolution 300 UV-spectrophotometer model with 10 mm matched quartz cell was used for all the absorbance measurements. 0.03 g of each sample was taken and placed in the quartz cell with 3.0 ml of pyridine in cyclohexane with initial concentration ≈1.2 mmol/l, the cell was covered with fitted quartz cover. The absorbance was measured as a function of time intervals from 1 to 270 min and measured each 5 min. The amount of adsorbed pyridine (mmol g^{-1}) was measured by means of Beer's law as the follow: $A = C \times \varepsilon \times l$ where, A = initial absorbance − measured absorbance. So, the amount of adsorbed pyridine (C) = $[A/\varepsilon \times l] \times (3/0.03)$ (mmol g^{-1}). The calcined samples were subjected to a Pyridine (Py) adsorption analysis in a Fourier transform infrared (FTIR) PerkinElmer Spectrum 100 spectrometer. The analysis was carried out over samples disc which was treated under vacuum at 1.33×10^{-3} Pa at room temperature. Later, the samples were treated with pyridine vapor and finally heated at 150 °C under high vacuum for 30 min. The amount of Brönsted and Lewis acid sites was calculated via integration of the area of the IR spectral absorption bands showing the maximum values of intensity at 1445 and 1542 cm^{-1}, respectively.

2.3. Catalytic activity measurements

The catalytic reaction was carried out in a fixed-bed, flow type reactor with a flow system under atmospheric pressure. A 0.30 g catalyst sample was packed into a quartz reactor. Ethanol was carried by purified N_2 as a carrier gas (5 mol% in N_2) by an evaporator–saturator, placed in a thermostat. The total flow rate of ethanol in the feed gas stream was 1.5 L/h. The catalyst was heated up to 300 °C at the rate of 100 °C/h and activated in N_2 for 3 h. All the reactions were carried out according to the same procedure where the catalyst was heated at a rate of 1 °C min^{-1} to the reaction temperature. The products were analyzed by means of Varian CP-3800 gas chromatograph, Agilent technologies (USA).

The percentage conversion of ethanol and the selectivity towards ethylene are defined as follows:

$$\text{percentage conversion of ethanol} = \frac{\text{amount of ethanol converted/h}}{\text{amount of ethanol fed/h}} \times 100$$

$$\text{percentage selectivity of ethylene} = \frac{\text{amount of ethylene formed/h}}{\text{amount of ethanol converted/h}} \times 100$$

Table 1
TGA and DSC data for dried H_3PMo, Ag_1PMo, Ag_2PMo and Ag_3PMo samples.

Sample	TGA data								DSC data		
	T_{max} of decomposition steps (°C)				No. of water molecules evolved/step				Endo-1 (°C)	Endo-2 (°C)	Exo-3 (°C)
H_3PMo[a]	129.45	240.32	351.64	420.10	10	2	1.5	–	182.38	360.80	385.32
Ag_1PMo	132.70	273.25	389.12	443.34	4.5	2.5	1	1	243.60	301.20	460.20
Ag_2PMo	124.18	234.70	357.40	451.13	1.5	3	2	0.5	243.90	308.10	475.67
Ag_3PMo	164.51	268.30	–	–	2.5	0.5	–	–	135.81	238.40	500.85

[a] Ref. [15].

3. Results and discussion

3.1. TG and DSC analysis

The data collected from TG and DSC experiments for all the samples are presented in Table 1. The TG data for H_3PMo sample reveals the presence of four steps of weight loss with temperature maxima located at 129.45, 240.32, 351.64 and 420.1 °C. During the TG analysis, physically adsorbed water and water of hydration evolved first, leaving anhydrous Keggin units with associated protons at temperature up to 351 °C. As the temperature increase gradually, the protonic water was evolved at 420 °C. This water is formed by extraction of an oxygen atom from the Keggin anion by two protons, thus decomposing the heteropoly Keggin structure. These observations are in agreement with the previous reports [7,15] that thermal treatment beyond 420 °C causes the decomposition of the Keggin structure of H_3PMo.

Ion exchange of protons with Ag resulted distinct weight losses. As-synthesized Ag_1PMo and Ag_2PMo catalysts showed four weight losses very similar to H_3PMo sample. However, only two weight losses were observed for as-synthesized Ag_3PMo sample corresponding to the removal of three water molecules with maximum temperature located at 164.5 °C and 268.3 °C. The dehydration pathways of H_3PMo and its silver substituted salts were illustrated in the following scheme.

$$\begin{aligned}
&H_3PMo_{12}O_{40}\cdot 12H_2O \xrightarrow{129.45\,^{\circ}C} H_3PMo_{12}O_{40}\cdot 2H_2O + 10H_2O\\
&H_3PMo_{12}O_{40}\cdot 2H_2O \xrightarrow{240.32\,^{\circ}C} H_3PMo_{12}O_{40} + 2H_2O\\
&H_3PMo_{12}O40 \xrightarrow{351.64\,^{\circ}C} PMo_{12}O_{38.5} + 1.5H_2O\\
&PMo_{12}O_{38.5} \xrightarrow{420.1\,^{\circ}C} 12MoO_3 + 0.5P_2O_5
\end{aligned} \quad \text{(i)}$$

$$\begin{aligned}
&AgH_2PMo_{12}O_{40}\cdot 9H_2O \xrightarrow{132.70\,^{\circ}C} AgH_2PMo_{12}O_{40}\cdot 4.5H_2O + 4.5H_2O\\
&AgH_2PMo_{12}O_{40}\cdot 4.5H_2O \xrightarrow{273.25\,^{\circ}C} AgH_2PMo_{12}O_{40}\cdot 2H_2O + 2.5H_2O\\
&AgH_2PMo_{12}O_{40}\cdot 2H_2O \xrightarrow{389.12\,^{\circ}C} AgH_2PMo_{12}O_{40}\cdot H_2O + H_2O\\
&AgH_2PMo_{12}O_{40}\cdot H_2O \xrightarrow{443.34\,^{\circ}C} AgH_2PMo_{12}O_{40} + H_2O
\end{aligned} \quad \text{(ii)}$$

$$\begin{aligned}
&Ag_2HPMo_{12}O_{40}\cdot 7H_2O \xrightarrow{124.18\,^{\circ}C} Ag_2HPMo_{12}O_{40}\cdot 5.5H_2O + 1.5H_2O\\
&Ag_2HPMo_{12}O_{40}\cdot 5.5H_2O \xrightarrow{234.70\,^{\circ}C} Ag_2HPMo_{12}O_{40}\cdot 2.5H_2O + 3H_2O\\
&Ag_2HPMo_{12}O_{40}\cdot 2.5H_2O \xrightarrow{357.40\,^{\circ}C} Ag_2HPMo_{12}O_{40}\cdot 0.5H_2O + 2H_2O\\
&Ag_2HPMo_{12}O_{40}\cdot 0.5H_2O \xrightarrow{451.13\,^{\circ}C} Ag_2HPMo_{12}O_{40} + 0.5H_2O
\end{aligned} \quad \text{(iii)}$$

$$\begin{aligned}
&Ag_3PMo_{12}O_{40}\cdot 3H_2O \xrightarrow{164.51\,^{\circ}C} Ag_3PMo_{12}O_{40}\cdot 0.5H_2O + 2.5H_2O\\
&Ag_3PMo_{12}O_{40}\cdot 0.5H_2O \xrightarrow{268.30\,^{\circ}C} Ag_3PMo_{12}O_{40} + 0.5H_2O
\end{aligned} \quad \text{(iv)}$$

The thermal events accompanying the heat treatment of H_3PMo and Ag substituted samples were followed up non-isothermally using differential scanning calorimetry (DSC).

DSC data of H_3PMo (Table 1) showed two endothermic peaks at 182.4 °C and 360.8 °C due to the loss of adsorbed water and crystallization water, respectively. In addition to these peaks, DSC of H_3PMo also showed one exothermic peak at 385.3 °C due to the decomposition of H_3PMo. DSC of Ag_1PMo and Ag_2PMo samples also showed endothermic peaks in the range of 240 °C and 300 °C which may be due to loss of crystalline water and these observations are in good agreement with the TGA results. An exothermic peak due to decomposition of Keggin ion was observed in Ag_1PMo and Ag_2PMo samples at 460 °C and 475 °C respectively. The Ag_3PMo sample showed two endothermic peaks relatively at low temperatures (135 °C and 238 °C) than Ag_1PMo and Ag_2PMo samples. Gurgul et al. [13] reported that the structure of Ag_3PMo salt loses the water hydrating Ag in the range of 100–200 °C. It is noteworthy that the thermal stability of the Ag salts is increasing with the increase of Ag content. A similar phenomenon was observed in case of Cs incorporated 12-tungstophosphoric acid catalysts [17].

The observed higher thermal stability of AgPMo samples could be ascribed to the partial substitution of protons by large monovalent Ag cations. This is possibly due to that the larger cations can coordinate to more oxygen atoms on the periphery of Keggin structure and consequently cause atoms in Keggin anion to have less mobility, which could stabilize the Keggin ion [18].

3.2. X-ray powder diffraction (XRD)

The powder X-ray diffraction patterns of the H_3PMo and Ag substituted H_3PMo calcined at 300 °C were presented in Fig. 1. The XRD pattern of the H_3PMo was similar as previously reported for the acid phase [19]. The diffraction patterns of AgPMo samples showed the existence of single crystalline phase corresponding to Ag salt of H_3PMo, which indicating the formation of homogeneous heteropoly Ag salt. The patterns assigned to the Keggin salts are shifted in comparison with the pure H_3PMo, towards the lower 2θ values. The lattice parameters calculated from XRD Keggin pattern (Fig. 2) are shifted towards higher values with the increase in the Ag cation content ranging from $a = 11.4146$ for Ag_1PMo salt to $a = 11.4978$ for Ag_3PMo salt. As shown in the thermal analysis, the AgPMo samples are less hydrated than the pure acid.

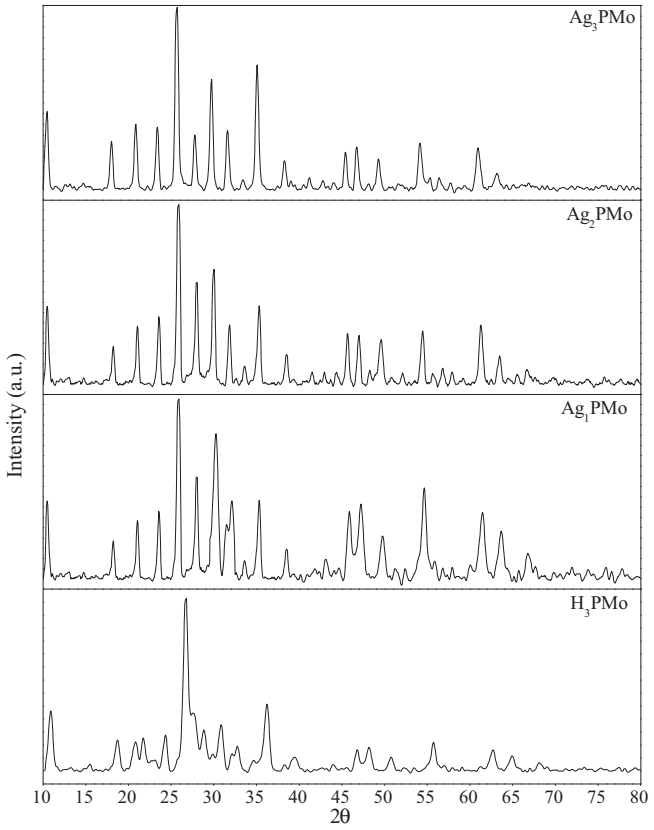

Fig. 1. XRD patterns of H_3PMo, Ag_1PMo, Ag_2PMo and Ag_3PMo catalysts.

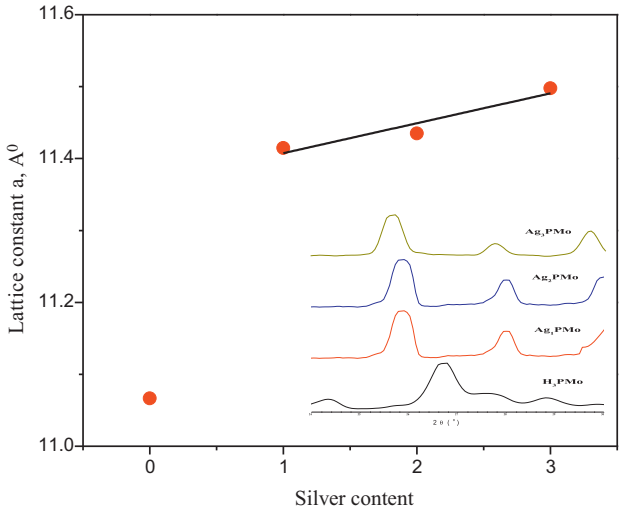

Fig. 2. Lattice constant as a function of the composition of AgPMo samples.

Substitution of the protons by these other cations caused a rearrangement of the secondary structure. This behaviour of decreasing cell parameters was observed for mono-valent (K^+, NH_4^+, Cs^+ and Rb^+) HPAs and has been extensively described in the literature [17,20,21].

The exchange of acidic protons present in the secondary heteropolyacid structure in the form of dihydronium ions for hydrated Ag cations is responsible for the contraction of the unit cell parameters [22]. Therefore the observed expansion in the lattice parameters upon increasing the Ag cation substitution is related to the decrease in the hydration of Ag salts as complemented by the postulated dehydration processes from thermal analysis data.

3.3. Fourier transformed infrared (FTIR) and Raman spectroscopy

The FTIR spectra for H_3PMo, Ag_1PMo, Ag_2PMo and Ag_3PMo samples calcined at 300 °C shown in Fig. 3. The presence of four characteristic bands for Keggin ion in the range of 700–1100 cm^{-1} can be observed in all the spectra. These bands are located at 1065, 960, 870 and 790 cm^{-1} which can be assigned to ν_{as}(P–O_a), ν_{as}(Mo–O_t), ν_{as}(Mo–O_b–Mo) and ν_{as}(Mo–O_c–Mo), respectively.

It is reported that substitution of any transition metal ion in place of Mo in the Keggin anion, induces the alterations in infrared spectrum that allow monitoring the presence of the metal inside the Keggin structure [23]. The previous reports also revealed that substituted metal induces a decrease of the oxoanion symmetry, leading to a split of the asymmetric (P–O_a) stretching band. As a consequence, a shoulder should be observed in the (P–O_a) band of the Ag incorporated samples. The FTIR spectral data of Ag incorporated samples did not showed any splitting of bands after Ag incorporation. This observation indicating that Ag metal ions did not replace the Mo in peripheral positions in Keggin anion, but they were substituted in place of the protons in the secondary structure of HPA. The shift of Mo–O_b–Mo vibration band at 870 cm^{-1} to higher wave numbers was observed in case of Ag_2PMo and Ag_3PMo samples. This is possibly resulting from high degree of Ag substitution leading to the opening of the structure of Keggin anion.

Raman technique is known to be well suited for observation of Keggin structures [24] to prove the presence of heteropolyacid structures. Fig. 4 represents the Raman spectra of H_3PMo and AgPMo samples calcined at 300 °C. The Raman spectrum for H_3PMo shows bands at 996, 983, 882, 603, and 246 cm^{-1} corresponding to ν_s(Mo–O_t), ν_{as}(Mo–O_t), ν_s(Mo–O_b–Mo), ν_s(Mo–O_c–Mo) and ν_s(Mo–O_a) modes respectively [25]. The Raman spectra of AgPMo samples showed bands at 999, 992, 883, 619, 606, 250 and 240 cm^{-1} that were assigned to $[PMo_{12}O_{40}]^{3-}$ ion. The differences in vibrational wavenumbers can be explained by the fact that the negative charge of polyanion is delocalized among a large number of oxygen sites (Mo–O_t bonds) in case AgPMo samples [26]. Also, it is known that the electrostatic interactions of Keggin anion-Ag were weaker than the Keggin anion–proton interactions. This behaviour could be attributed to the smaller ionic radius of hydrogen compared to Ag; as a result, the hydrogen charge density is greater, increasing the electrostatic interaction.

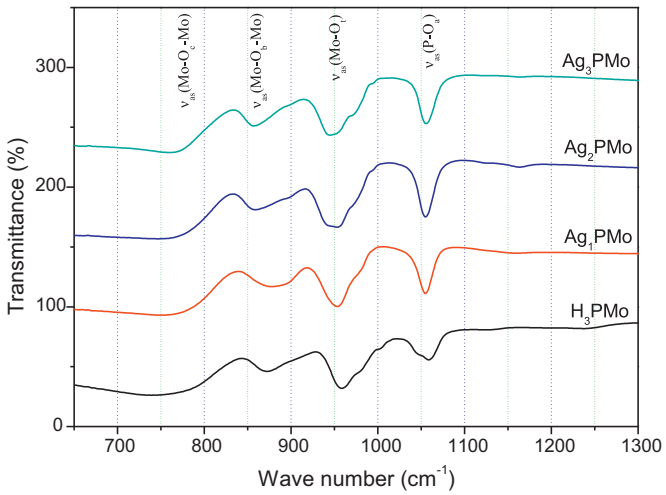

Fig. 3. FTIR spectra of H_3PMo and AgPMo samples.

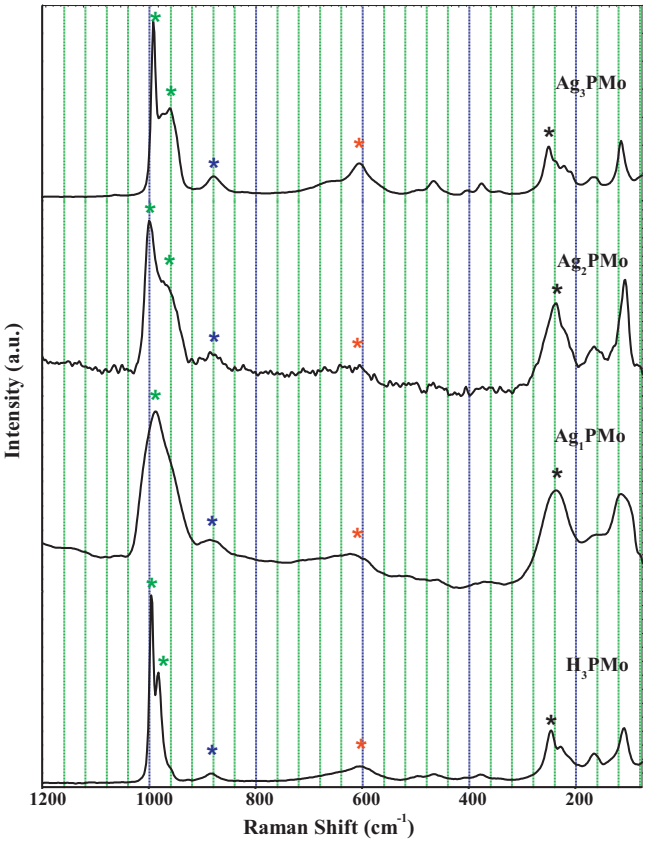

Fig. 4. Raman spectra of H_3PMo and AgPMo samples.

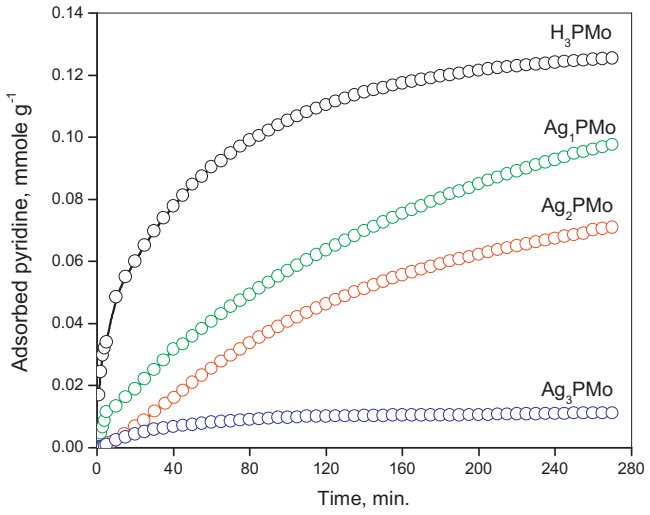

Fig. 5. Pyridine adsorption isotherms for H_3PMo and AgPMo samples.

3.4. Acidity of catalysts by pyridine adsorption

In order to assess the effect of the degree of Ag substitution on the total acidity of the H_3PMo, pyridine adsorption measurement were performed. The amount of pyridine adsorbed for the H_3PMo and their silver substituted salts were plotted against time intervals from 1 to 270 min. Adsorption of pyridine over these samples resemble to chemisorption of pyridine isotherm as a result of a chemical reaction between pyridine and Brönsted and Lewis acid sites presented in the sample.

Fig. 5 illustrates the amount of adsorbed pyridine (mmol g^{-1}) against time intervals from 1 to 270 min. over all the investigated samples calcined at 300 °C. Generally, the amount of adsorbed pyridine increases as the time intervals increases, and the amount of adsorbed pyridine for all the samples was maximized at 270 min. The adsorption of pyridine on H_3PMo sample is similar to chemisorption phenomena and therefore, the completion of a unimolecular adsorbed layer at the end of the experiment time was achieved (i.e. at 270 min.). Sufficient time and higher concentration of pyridine could be required to attain the unimolecular adsorption.

Ag_1PMo and Ag_2PMo samples were adsorbed excess amount of pyridine which reveals the high acidity of these samples. These samples have not reached to the completion of a unimolecular adsorbed layer. On the other hand, Ag_3PMo sample, reach to the completion of a unimolecular adsorbed layer at 100 min. These results indicating that the acidity presented in the Ag_3PMo is only due to presence of Lewis acid sites. The order of acid strength of the catalysts can be arranged as the follows: $H_3PMo > Ag_1PMo > Ag_2PMo > Ag_3PMo$.

The adsorbed pyridine is frequently analyzed by FTIR spectroscopy to distinguish the different acid sites presented in the samples [27].

FTIR pyridine adsorption spectra of the H_3PMo and AgPMo samples are shown in Fig. 6. The spectra showed sharp pyridine absorption bands at 1445, 1489, 1542, 1603 and 1636 cm^{-1}. The peaks at 1445 and 1603 cm^{-1} were due to the interaction of pyridine with Lewis acidic sites, while the peaks at 1542 and 1636 cm^{-1} were due to the protonation of pyridine molecule by the Brönsted acid sites [28]. The peak at 1489 cm^{-1} was due to the vibration of pyridine adsorbed on Brönsted acidic sites and on Lewis acidic sites [28]. The small hump presented in all the samples at 1583 cm^{-1} represents physically adsorbed pyridine.

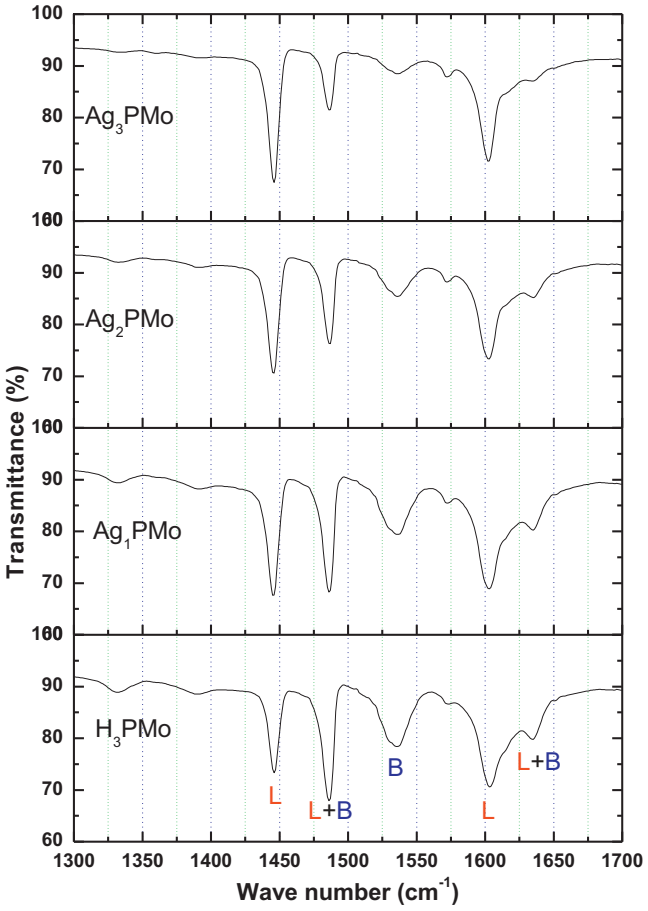

Fig. 6. FTIR spectra of samples after pyridine adsorption.

H_3PMo samples possessed strong Brönsted and Lewis acidic sites. With the increase of Ag content, the intensity of the peak due to only Brönsted acid sites at 1542 cm^{-1} was reduced. In contrast, the intensity of the peak due to Lewis acidic sites at 1445 cm^{-1} was increased with increase of Ag content.

Acidic properties of the heteropoly compounds in the solid state are sensitive to counter cations constituent elements of polyanions, and tertiary structure. Partial hydrolysis and in homogeneity of composition brought about during preparation are also important in governing the acidic properties; there are several possible types of origins of acidity [29].

1. Dissociation of coordinated water;

$$[M(H_2O)_m]^{n+} \rightarrow [M(H_2O)_{m-1}(OH)]^{(n-1)} + H^+$$

2. Lewis acidity of metal ions

Table 2
Pyridine adsorption data for the samples.

Sample	Data from FTIR pyridine adsorption		B/L ratio
	Peak- B	Peak- L	
H_3PMo	4562.46	2169.54	2.10
Ag_1PMo	3872.71	2886.69	1.34
Ag_2PMo	3346.49	3536.07	0.95
Ag_3PMo	3049.29	3706.69	0.82

3. Protons formed by the reduction of metal ions;

$$Ag^{+} + \tfrac{1}{2}H_2 \rightarrow Ag^{0} + H^{+}$$

4. Protons present in acidic salts

The ratio of Brönsted (B) and Lewis (L) acid sites, obtained from the peak area under absorption peaks at 1542 and 1445 cm^{-1} [30] were tabulated in Table 2. With increase of Ag content from 0 to 3, the B/L ratio decreased from 2.1 to 0.82. These results clearly show that substitution of Ag in place of protons caused the decrease in the Brönsted acidic strength of the samples. Increase of Ag content in the samples reflected the increase of Lewis acidity due to presence of Ag^{+} ions.

3.5. Dehydration of ethanol activity

The plot of overall ethanol conversion against the reaction temperature for all the investigated catalysts is shown at Fig. 7. The main products of ethanol dehydration reaction were ethylene and diethyl ether. The percentage conversion of ethanol increases with increasing the reaction temperature from 200 °C to 300 °C for all investigated catalysts. The catalytic activity of catalysts could be arranged in the order; $H_3PMo > Ag_2PMo > Ag_1PMo > Ag_3PMo$. H_3PMo sample offered high conversion at different reaction temperatures; however Ag_2PMo catalyst also showed almost equal conversion (93.05%) at 300 °C. The conversion of ethanol is clearly depended on the acidity of the catalysts. The higher amounts of Ag cations substituted in the H_3PMo, the lower the acidity of the catalysts. Herrera et al. [31] and Varisli et al. [32] also observed that presence of Brönsted acid sites is the major indication of the activity of the catalysts in alcohol dehydration reactions. The exceptional behaviour of Ag_2PMo catalyst could possibly due to high mobility of the protons.

Fig. 8 illustrates the % selectivity over the investigated catalysts. It was found that H_3PMo catalyst offered the high selectivity towards diethyl ether. In contrast, Ag substituted salt catalysts showed high % selectivity towards the formation of ethylene. The % selectivity to ethylene increased with increasing the reaction temperature from 200 to 300 °C. In this temperature range, the dehydration of ethanol to ethylene was the main reaction, where the high selectivity to ethylene was observed for Ag_2PMo sample and H_3PMo showed poor ethylene selectivity.

Blaszkowski and Van Santen [33] studied the mechanism of dimethyl ether formation from methanol over proton containing zeolite catalysts and revealed that dimethyl ether formation on zeolites was expected to take place by the reaction of the $[CH_3{\cdot}OH_2]^{+}$ and $[CH_3O]^{-}$ surface species, which were adsorbed on the Brönsted acid sites. As expected H_3PMo catalyst offered high selectivity to diethyl ether due to the fact that it possessed more number of Brönsted acid sites (Table 2).

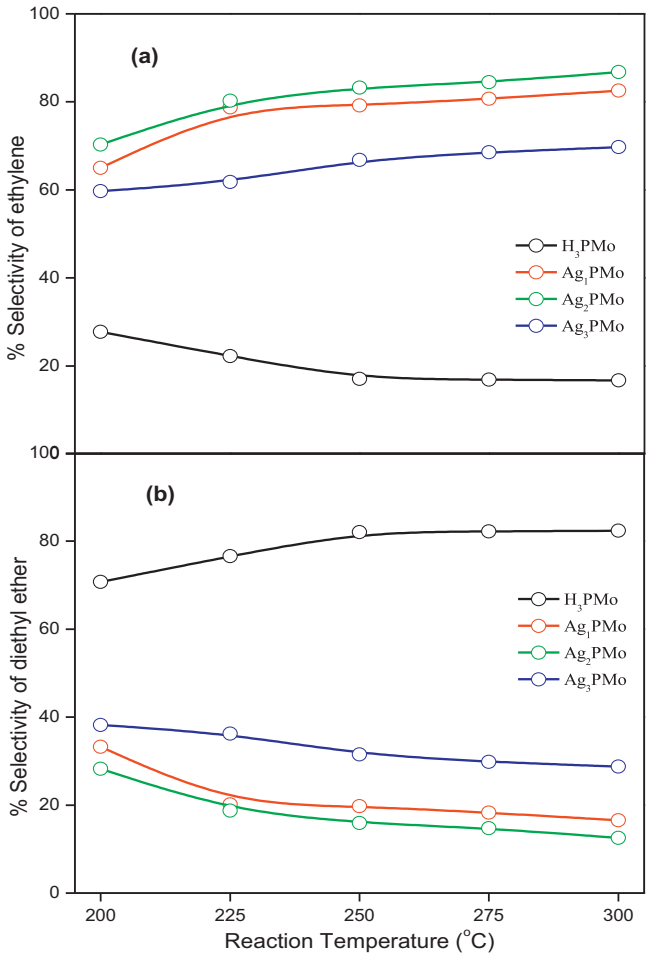

Fig. 8. Effect of reaction temperature on: (a) % selectivity towards ethylene, (b) % selectivity towards diethyl ether.

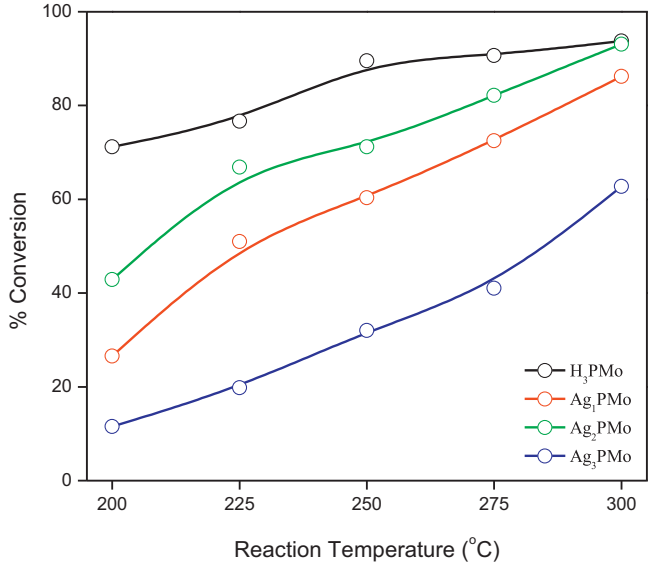

Fig. 7. Effect of reaction temperature on % conversion of ethanol over all catalysts.

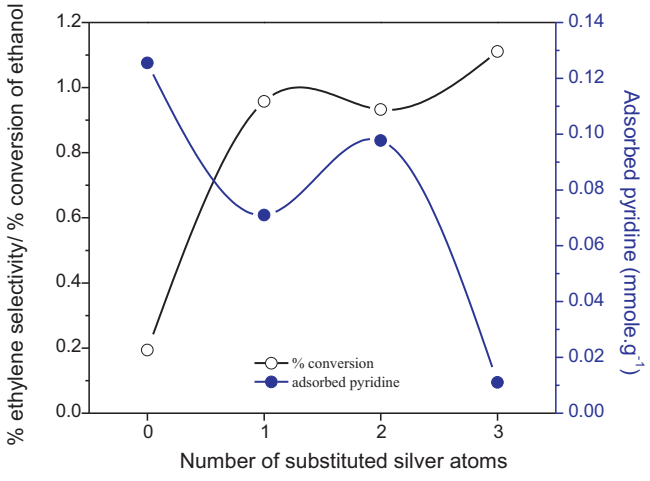

Fig. 9. % ethylene selectivity/% conversion of ethanol and pyridine adsorption versus number of substituted silver atoms of catalysts at 300 °C reaction temperature.

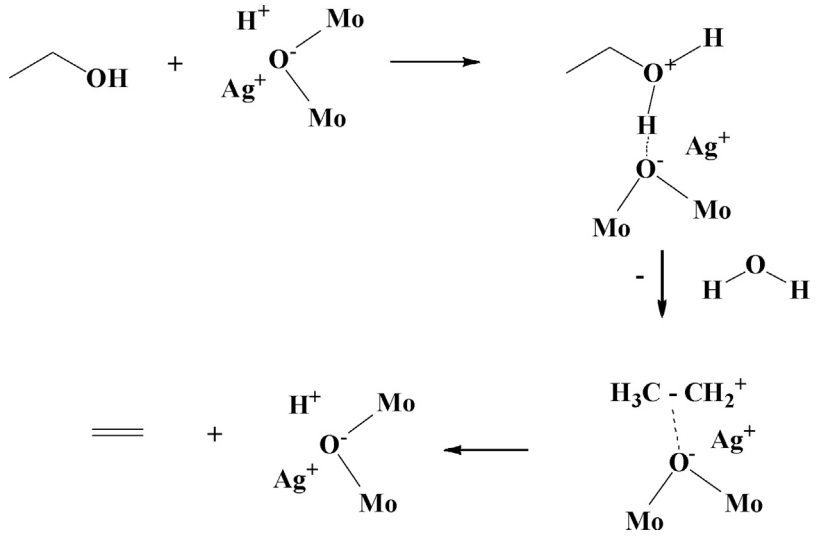

Scheme 1. Plausible reaction pathway of ethanol dehydration over $Ag_xH_{3-x}PMo_{12}O_{40}$ catalysts.

A correlation between the % ethylene selectivity/% conversion of ethanol, the corresponding total acidity and the degree of substitution order of Ag cation was examined and plotted in Fig. 9. It is clear from this figure that Ag_3PMo catalyst showed maximum % selectivity/% conversion. The general trend of % ethylene selectivity/% conversion of ethanol could be arranged in the order $Ag_3PMo > Ag_1PMo \geq Ag_2PMo > H_3PMo$.

The high % selectivity/% conversion for Ag substituted samples could be explained by the fact that the generation of additional protons from water coordinated to Ag cations. Haber et al. [6] reported that heating of $Ag_xH_{3-x}PW_{12}O_{40}$ salts at about 250 °C caused the release of water hydrating protons from Ag-coordinated water. The water coordinated to Ag cations increases with increase of Ag incorporation. The authors also noticed that the protons generated by dissociation of water coordinated to the Ag atoms influences the yield of the ethylene, more the coordinated water and more the ethylene formed. The catalytic activity data is revealing that a similar phenomenon is taking place in case of AgPMo samples.

A plausible mechanism (Scheme 1) for the dehydration reaction could be proposed in the light of dissociation–rehydration cycle on the active sites of Ag substituted heteropoly salts.

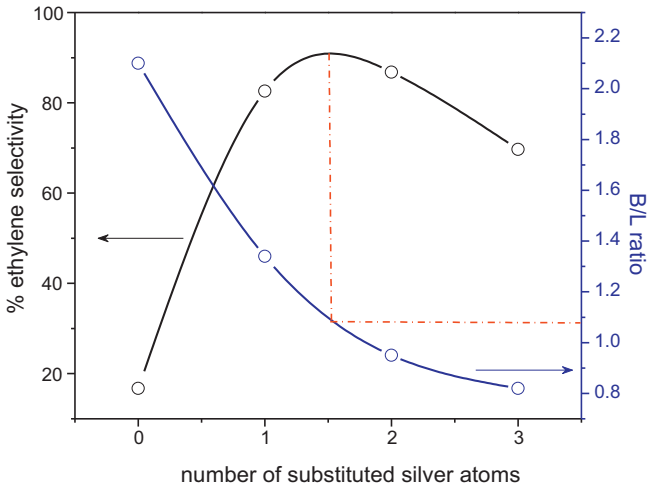

Fig. 10. % ethylene selectivity and B/L ratio versus number of substituted silver atoms of catalysts at 300 °C reaction temperature.

An attempt has made to draw a correlation between number of Ag atoms presented in the sample and B/L ratio and its subsequent affect on the ethylene selectivity (Fig. 10). It is clear that number of Ag ions have great influence on the acidity nature and selectivity to ethylene. It appears that maximum ethylene selectivity can be obtained with the catalyst which possessed B/L ratio around 1.1.

4. Conclusions

The Ag salts of 12-molybdophosphoric acid in the whole range $0 < x < 3$ were synthesized. The Keggin structure of the prepared salts was thermally stable above 450 °C. The XRD measurements showed that Ag salts are in the single crystalline phase. FTIR pyridine adsorption measurements were used to determine the Brönsted and Lewis acid sites presented in the samples. Dehydration of ethanol into ethylene and diethyl ether was investigated over 12-molybdophosphoric acid and $Ag_xH_{3-x}PMo_{12}O_{40}$ catalysts. 12-Molybdophosphoric acid was the most active catalyst for the dehydration of ethanol; however it offered poor selectivity to ethylene. The conversion of ethanol is depended on the Brönsted acidity of the catalysts. The Ag_2PMo catalyst with the largest amount of coordinated water shows the highest selectivity towards ethylene formation. The correlation between Brönsted acid sites/Lewis acid ratio and ethylene selectivity was obtained and it appears that equal number Brönsted and Lewis acids would help to obtain high ethylene selectivity.

Acknowledgments

This project was funded by the Deanship of Scientific Research (DSR), King Abdulaziz University, Jeddah, under grant no. (133-130-D1432). The authors, therefore, acknowledge with thanks DSR technical and financial support.

References

[1] V.V. Bokade, G.D. Yadav, Applied Clay Science 53 (2011) 263.
[2] Y. Gucbilmez, T. Dogu, S. Balci, Industrial and Engineering Chemistry Research 45 (2006) 3496.
[3] C.J. Pereira, Science 285 (1999) 670.
[4] T. Kito- Borsa, S.W. Cowley, Division of Energy & Fuels 49 (2) (2004) 856.
[5] I. Takahara, M. Saito, M. Inaba, K. Muruta, Catalysis Letters 105 (2005) 249.
[6] J. Haber, K. Pamin, L. Matachowski, B. Napruszewska, J. Poltowicz, Journal of Catalysis 207 (2002) 296.

[7] P. Vázquez, L. Pizzio, C. Cáceres, M. Blanco, H. Thomas, E. Alesso, L. Finkielsztein, B. Lantano, G. Moltrasio, J. Aguirre, Journal of Molecular Catalysis A: Chemical 161 (2000) 223.
[8] J.D. Varisli, T. Dogu, G. Dogu, Chemical Engineering Science 62 (2007) 5349.
[9] A. Ciftci, D. Varisli, K.C. Tokay, N.A. Sezgi, T. Dogu, Chemical Engineering Journal 207–208 (2012) 85.
[10] S. Suzuki, S. Kogai, Y. Ono, Chemistry Letters 13 (1984) 699.
[11] H. Niiyama, Y. Saito, S. Yoshida, E. Echigoya, Nippon Kagaku Kaishi 1982 (1982) 569.
[12] T. Baba, H. Watanabe, Y. Ono, Journal of Physical Chemistry 87 (13) (1983) 2406.
[13] J. Gurgul, M. Zimowska, D. Mucha, R.P. Socha, L. Matachowski, Journal of Molecular Catalysis A: Chemical 351 (2011) 1.
[14] L. Matachowski, M. Zimowska, D. Mucha, T. Machej, Applied Catalysis B 123–124 (2012) 448.
[15] T.T. Ali, S.A. Al-Thabaitib, A.O. Alyoubib, M. Mokhtar, Journal of Alloys and Compounds 496 (2010) 553.
[16] B.W.L. Southward, J.S. Vaughan, C.T. O'Connor, Journal of Catalysis 153 (1995) 293.
[17] K. Narasimharao, D.R. Brown, A.F. Lee, A.D. Newman, P.F. Siril, S.J. Tavener, K. Wilson, Journal of Catalysis 248 (2007) 226.
[18] K. Na, T. Okuhara, M. Misono, Journal of the Chemical Society, Faraday Transactions 91 (2) (1995) 367.
[19] S. Damyanova, J.L.G. Fierro, Chemistry of Materials 10 (1998) 871.
[20] A. Corma, A. Martinez, C. Martinez, Journal of Catalysis 164 (1996) 422.
[21] J.A. Dias, E. Caliman, S.C.L. Dias, Microporous and Mesoporous Materials 76 (2004) 221.
[22] J. Thiel, C. Ritchie, H.N. Miras, C. Streb, S.G. Mitchell, T. Boyd, M. Nieves, C. Ochoa, M.H. Rosnes, J. McIver, D. Long, L. Cronin, Angewandte Chemie International Edition 49 (2010) 6984.
[23] C. Marcha-Roch, N. Laronze, N. Guillou, A. Teze, G. Herve, Applied Catalysis A: General 199 (2000) 33.
[24] A. Bruckner, G. Scholz, D. Heidemann, M. Schneider, D. Herein, U. Bentrup, M. Kant, Journal of Catalysis 245 (2007) 369.
[25] A. Anzai, K. Inumaru, S. Yamanaka, Journal of Alloys and Compounds 432 (2009) 557.
[26] J.M. Poblet, X. Lopez, C. Bo, Chemical Society Reviews 32 (2003) 297.
[27] M.N. Timofeeva, Applied Catalysis A: General 256 (2003) 19;
K. Okumura, K. Yamashita, M. Hirano, M. Niwa, Journal of Catalysis 234 (2005) 300.
[28] B.M. Devassy, F. Lefebvre, S.B. Halligudi, Journal of Catalysis 231 (2005) 1.
[29] C.R. Deltcheff, M. Fournier, R. Franck, R. Thouvenot, Inorganic Chemistry 22 (1983) 207;
M.K. Shane, C.B. Tervor, C.B. Robert, Catalysis Today 131 (2008) 526;
T. Baba, J. Sakai, Y. Ono, Bulletin of the Chemical Society of Japan 55 (1982) 2633.
[30] B.H. Davis, R.A. Keogh, S. Alerasool, D.J. Zalewski, D.E. Day, P.K. Doolin, Journal of Catalysis 183 (1999) 45.
[31] J.E. Herrera, J.H. Kwak, J.Z. Hu, Y. Wang, C.H.F. Peden, Topics in Catalysis 49 (2008) 259.
[32] D. Varisli, T. Dogu, G. Dogu, Industrial and Engineering Chemistry Research 48 (2009) 9394.
[33] S.R. Blaszkowski, R.A. Van Santen, Journal of the American Chemical Society 118 (1996) 5152.